

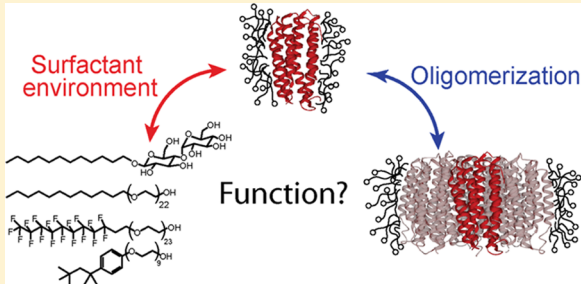
Proteorhodopsin Function Is Primarily Mediated by Oligomerization in Different Micellar Surfactant Solutions

Matthew N. Idso,[†] Naomi R. Baxter,[‡] Sirish Narayanan,[‡] Evelyn Chang,[‡] Julia Fisher,[†] Bradley F. Chmelka,[†] and Songi Han^{*,†,‡,§}

[†]Department of Chemical Engineering and [‡]Department of Chemistry and Biochemistry, University of California, Santa Barbara, Santa Barbara, California 93106, United States

Supporting Information

ABSTRACT: The diverse functionalities of membrane proteins (MPs) have garnered much interest in leveraging these biomolecules for technological applications. One challenge of studying MPs in artificial micellar surfactant environments is that many factors modulate their structures and functionalities, including the surfactants that interact with the MP or their assembly into oligomers. As oligomerization offers a means by which MPs could selectively interact among the copious environmental factors in biological environments, we hypothesized that MP function is predominantly modified by oligomerization rather than interactions with local surfactants that, by comparison, largely interact with MPs nonspecifically. To test this, we study the light-activated proton pump proteorhodopsin (PR) in micellar surfactant solutions because it is functionally active in monomeric and oligomeric forms, the light-activated functionalities of which can be assessed in detail. The surfactant composition and oligomerization are correlated with PR function, as measured by the protonation behaviors of aspartic acid residue 97, which mediates light-activated proton transport, and the associated photocycle kinetics. The results demonstrate that oligomerization dominantly mediates PR function in different surfactant environments, whereas some surfactants can subtly modulate proton-pumping kinetics. This work underscores the importance of understanding and controlling oligomerization of MPs to study and exploit their function.



INTRODUCTION

Membrane proteins (MPs) are biomacromolecules with functionalities that impart transport,^{1–3} catalytic,^{4,5} sensing,⁶ and structural⁷ properties to biological lipid membranes to facilitate cellular functions. Such proteins have extensive hydrophobic transmembrane regions that interact with surfactants (e.g., lipids or detergents), as well as other protein constructs, which can result in the formation of oligomeric protein assemblies^{8–11} that are typically held together by weak interactions. Numerous studies have shown that an MP oligomer can exhibit enhanced protein stability,^{12–14} modified protein function,^{8,15–18} or more complex functional properties compared to its monomeric subunits.^{19,20} Due to the importance of MP oligomerization, researchers have recently employed powerful characterization techniques, including electron paramagnetic resonance or nuclear magnetic resonance (NMR) spectroscopy, to interrogate the oligomeric structures of MPs at the molecular level.^{21–23} Some studies also suggest that the surfactant environment plays a significant role in adjusting MP function.^{15,23–27} Still, studies that directly address the question of whether MP function is dominantly and directly tuned by oligomerization are lacking, although clarifying this question is an important goal. A key challenge in comparing the functional roles of oligomerization and local surfactant environments is that these factors are often

interdependent,^{12,15} making it difficult to distinguish their effects on protein function.

In a biological context, the protein-specific interactions of MP oligomers could serve to selectively perturb protein characteristics amidst the copious environmental factors (i.e., lipids, salts, water, etc.) present in cellular lipid bilayer environments. Therefore, we hypothesize that oligomerization exerts a dominant functional influence on MPs, as opposed to local surfactant interactions, which by comparison are largely hydrophobic and nonspecific. To test this hypothesis, we selected an MP system in which (1) the surfactant environment and relative monomer and oligomer populations can be separately adjusted while retaining protein function and (2) changes in the MP function can be correlated with the differences in oligomer distributions and surfactant environments. We chose to study the heptahelical transmembrane protein proteorhodopsin (PR), a proton-pumping eubacterial rhodopsin,^{28–30} solubilized in a micellar surfactant solution. In these systems, surfactants associate with the MPs^{31,32} and exchange with surfactants in solution,³³ which should allow the surfactant composition near the protein surface to be adjusted

Received: January 30, 2019

Revised: March 27, 2019

Published: March 29, 2019

by the surfactant composition in the bulk solution. Moreover, surfactant-solubilized PR samples can be separately prepared as functional monomers or oligomers by size-exclusion chromatography (SEC)¹⁰ or by the use of point mutations, e.g., E50Q, that enrich the monomeric PR populations compared to the wild-type variant.²³ Finally, PR has a complex light-activated proton-pumping functionality³⁴ that yields functional information at a level of detail^{35,36} typically not available for many MPs.

In particular, Hussain et al. report that surfactant-solubilized PR monomers and oligomers exhibit substantially different photochemical reaction cycle kinetics, which are associated with PR's H⁺-transport process and the pK_a of the aspartic acid residue 97 (pK_{aD97}), a key moiety that mediates light-activated proton transport. Hussain et al. established that monomeric PR underwent an ~5 times faster photocycle and displayed a significantly higher pK_{aD97} value (pK_{aD97} = 7.4) than the oligomeric PR (pK_{aD97} = 6.7), with the difference proposed to arise from the presence/absence of an interprotein W34–H75 hydrogen bond,¹⁵ as identified by Ran et al.³⁷ These functional differences were relatively insensitive to the type of surfactant that solubilized the PR, specifically between *n*-dodecyl- β ,D-maltoside (DDM), *n*-dodecyl phosphocholine, and diheptanoyl-*sn*-glycero-3-phosphotidylcholine (diC₇PC).¹⁵ Subsequently, Maciejko et al.²³ reported similarly distinct pK_{aD97} values for hexameric PR in DDM (pK_{aD97} = 6.9) and monomeric PR in octylglucoside (pK_{aD97} = 8.0), consistent with that of Hussain et al.¹⁵ These researchers, however, also observed a surprisingly low pK_{aD97} of 6.9 for PR in monomeric Triton X-100 (TX100) surfactants.²³ Based on this observation, Maciejko et al.²³ suggested that some surfactants may be equally potent modifiers of PR function, which would contradict the hypothesis that interprotein interactions dominate functional regulation.

Our study takes this apparent contradiction as a starting point to test our stated hypothesis with a scope that extends that of the studies of both Hussain et al. and Maciejko et al.^{15,23} Functional analyses of monomeric and oligomeric PR in DDM surfactants help establish the degree to which oligomerization mediates the protonation behaviors of the functionally relevant D97 residue and the photocycle kinetics, providing a scale by which to compare the effects of the surfactant environment. The same functional parameters were acquired for PR in solutions of Triton X-100 (TX100), Brij-35, or the fluorinated Zonyl FSN-100 (Zonyl) surfactant micelles, as well as in mixtures of these surfactants with DDM, and subsequently correlated with the oligomeric distribution of PR species. The collective analyses reveal that oligomerization dominantly modifies PR function, relatively independent of the surfactant environments investigated here, whereas changes to the surfactant environment exert in some cases subtle effects on PR function.

■ EXPERIMENTAL SECTION

Sample Preparation. The expression and purification of green-absorbing PR were essentially carried out as described previously¹⁰ but with a few exceptions. Namely, additional freeze-fracture steps (three freeze–thaw cycles) were used to lyse the *Escherichia coli* cells and the lysed cell fragments were collected by centrifugation at ~7000g, rather than using ultracentrifugation. All protein purification steps were

performed in aqueous (aq) buffered solutions that consisted of 150 mM KCl and 50 mM K₂HPO₄, which provided a pH of ~8.7, and surfactant quantities are expressed as a weight-per-volume percent or in molarity. Green PR was cloned into a pET26b(+) plasmid vector containing an additional C-terminal HSV sequence and hexahistidine tag for purification. In addition, we used the triple-cysteine mutant of PR, in which the three natural cysteines are mutated to serine residues, to reduce variability in protein function as a result of cysteine oxidation and/or post-translational modifications;³⁵ we refer to this protein as cysteine-less (cys-less) PR throughout the article. Additional mutations were introduced to the cys-less green PR template vector via site-directed mutagenesis by polymerase chain reaction amplification with mutagenic primers. Vectors were transformed into *E. coli* XL1-Blue competent cells and were plated on Luria–Bertani (LB) agar plates containing kanamycin and subsequently grown at 37 °C overnight. Colonies were picked and grown in LB medium, and the plasmid DNA was isolated using a GeneJET Plasmid Miniprep Kit. Sequences were verified with GENEWIZ. Expression of cys-less and mutant green PR was carried out in *E. coli*-competent BL21 (DE3) cells in LB. Cells were grown to an OD₆₀₀ of 0.8–1 at which point expression was induced by the addition of isopropyl β -D-1-thiogalactopyranoside to a concentration of 1 mM, and retinal was added such that the final concentration was 10 μ M. Cell disruption and Ni-NTA matrix purification were performed, as described previously,¹⁰ except that a freeze-fracture technique using liquid nitrogen was employed, in addition to sonication to further lyse cell membranes. All samples were desalted with Sephadex G-25 M PD-10 Columns (GE Healthcare) prior to subjecting them to size-exclusion chromatography (SEC). SEC was used to isolate the different oligomeric forms of PR and assess the oligomeric state, as described by Stone et al.¹⁰ PR samples were purified in DDM, exchanged into D₂O by concentrating the PR-containing solution in a 50 kDa molecular weight cutoff centrifugal concentrator to a volume of ~300 μ L, and then mixed with a 0.1% DDM alkaline buffer made with D₂O (Cambridge isotopes, 98%) to achieve a final volume of ~1 mL.

Surfactant Exchange Protocol. To exchange the surfactants that solubilize PR, a solution with 0.5 mg of PR purified in DDM was added to ~10 mL of phosphate-buffered solution (50 mM KH₂PO₄, 150 mM KCl) containing an appropriate amount of Ni-NTA resin, such that all PR was bound. After PR was completely bound, the resin was allowed to settle and the supernatant was removed. The protein-bound resin was then washed with ~120 mL of phosphate buffer with the desired surfactant (0.1 wt %) by repeatedly resuspending the resin in 40 mL of solution, allowing the resin to settle (~15 min), and then removing the supernatant. Subsequently, the protein-bound resin was resuspended in an additional 40 mL of phosphate buffer with the desired surfactant (0.1 wt %) and incubated with shaking at 4 °C overnight (~18 h). Following the removal of the supernatant, the PR was eluted from the resin by incubation in 0.5–1 mL of phosphate-buffered solution with 500 mM imidazole and the desired surfactant (0.1 wt %) for ~30 min. Imidazole was removed by running the protein-containing solution through a PD-10 desalting column equilibrated in phosphate buffer with the desired surfactant (0.1 wt %). Solution-state ¹H NMR analyses (see below and Figure S1 of the Supporting Information (SI)) established the presence of only the desired surfactant in the

protein-containing solutions prepared by this surfactant exchange protocol.

Blue-Native Polyacrylamide Gel Electrophoresis (BN-PAGE). The distributions of proteorhodopsin monomers and oligomers in protein samples were assessed using BN-PAGE. Preparation and electrophoresis of BN-PAGE gels (Native-PAGE Novex Bis–Tris gel 4–16%, 10 wells) were performed according to manufacturer's instructions. Samples were prepared with 3–4 μg of the protein, 5 μL of the sample buffer, 1 μL of 5% Coomassie Brilliant Blue G250 solution, and H_2O adjusted to a total volume of 20 μL . Integration of signal intensities on BN-PAGE gels was carried out with ImageJ software using first a background subtraction (rolling ball method, 150 pixels) and then integrating along the direction of low to high molecular weight, averaging across the entire width of the respective lane. An example of the background-subtraction and integration processes used in this study is shown in Figure S2 of the SI.

Optical Absorption Measurements and Analyses. UV–visible absorption spectra of cys-less proteorhodopsin and E50Q variants were recorded using a Shimadzu UV-1800 spectrophotometer. The optical absorbance of each sample was recorded over a wavelength range of either 250–750 or 400–750 nm in increments of 0.5 nm. All samples had an initial volume of 750 μL , were buffered with 50 mM KCl and 150 mM K_2HPO_4 , and had optical densities of >0.15 at 520 nm. Samples were titrated with 1 M NaOH (aq) from the initial pH to a pH of 10 and then with 1 M HCl (aq) to a pH of 4. Approximately 30 μL of 1 M HCl or NaOH was used during the titration, so the ionic strength changed by ~ 30 mM during the measurement. The pH was measured using a low-volume pH probe (Mettler Toledo).

$pK_{a_{D97}}$ Analyses. The pK_a of the D97 residue side chain of proteorhodopsin was determined by analyses of the UV–visible absorption spectra. Briefly, each UV–visible absorption spectrum was adjusted by a zero-order baseline correction, such that the absorbance at 750 nm had zero intensity and was subsequently normalized to the maximum absorbance intensity between 510 and 550 nm to account for dilution. Then, the absorbance spectrum recorded at the most alkaline pH (~ 10) was subtracted from each spectrum to yield difference absorbance spectra. The difference absorbance at 570 nm was normalized and fitted to the Henderson–Hasselbalch equation^{38,39} using nonlinear least-squares regression and a home-constructed MATLAB code with two fitting parameters: the pK_a value and Hill coefficient (code available in the Supporting Information). We hypothesized that inter-PR interactions among oligomers could promote cooperative binding and so included a Hill coefficient to assess the binding cooperativity of PR in our $pK_{a_{D97}}$ analysis. The distribution of monomeric and oligomeric cys-less PR in DDM was not affected by incubation overnight (~ 18 h) under pH conditions ranging from 3 to 11 (Figure S3, SI). Also, only subtle differences in monomer and oligomer populations were observed for E50Q PR in various micellar surfactant solutions before and after implementing the pH titration protocol used to probe the protonation behaviors of D97 (Figure S3, SI). To test robustness, $pK_{a_{D97}}$ measurements were acquired on three samples of as-purified cys-less PR in DDM surfactants, which yielded standard deviations of ~ 0.05 and ~ 0.02 for the $pK_{a_{D97}}$ and Hill coefficients, respectively (Figure S4, SI). Based on

these measurements, we expect the errors in the $pK_{a_{D97}}$ and Hill coefficients to be approximately 0.1 and 0.05, respectively.

Flash Photolysis Measurements and Analyses. Flash photolysis measurements were conducted using a SpectraPhysics Nd:YAG laser with a monochromator. Samples were illuminated by a 10 ns 532 nm laser flash, and the transient absorbances at several wavelengths were monitored over a time span of 10 μs to ~ 0.5 s. For each wavelength measured, 5096 absorbance points were collected with time resolutions of 20 ns, 20 μs , and 2 ms and subsequently stitched together to yield an absorbance trace. Absorbance data at each wavelength was averaged over approximately 200 logarithmically spaced time points and was truncated below 40 μs to account for artifacts from the laser. Global fitting analyses were performed using a home-written MATLAB code (code available in the Supporting Information). The PR concentrations and pH of all samples characterized using flash photolysis measurements are shown in Table S1, Supporting Information.

Solution-State ^1H NMR. Solution-state ^1H single-pulse NMR measurements were used to quantify the surfactants in solutions without and with proteorhodopsin species. ^1H NMR measurements were conducted on a Varian NMR spectrometer operating at a field strength of 14.1 T, which corresponds to a ^1H Larmor frequency of 600 MHz. Samples were prepared by diluting 50 μL of the proteorhodopsin-containing solution in 950 μL of D_2O (Cambridge isotopes, 98%) in a 1-in-20 dilution. Each ^1H NMR measurement used an acquisition time of 6 s, a delay time of 10 s, and between 16 and 64 signal-averaging scans. The amounts of DDM surfactants in proteorhodopsin-containing solutions were determined by comparing the integrated areas of ^1H NMR peaks of DDM of spectra from the protein-containing solutions and a solution containing 0.1% (w/v) DDM in D_2O .

RESULTS AND DISCUSSION

To compare the effects of the surfactant environment and oligomerization on proteorhodopsin function, we employed a combination of complementary characterization methods to quantify the surfactant composition of the PR-solubilizing micellar solutions, to isolate monomeric and oligomeric PR species, and to gain insight into the distribution of PR monomers and oligomers in micellar solutions. Information derived from these techniques is correlated with PR function, including the protonation behaviors of the residue D97 and the photocycle kinetics of PR at microsecond time resolution as probed by time-resolved visible absorbance spectroscopy.

Selection of PR-Stabilizing Surfactants. The surfactants explored in this study were judiciously selected to span a range of molecular architectures to test whether the types of head group or tail moieties influence PR function. Specifically, this study explores the effects of *n*-dodecyl- β ,*D*-maltoside (DDM), Brij-35, Triton X-100 (TX100), and Zonyl FSN-100 (Zonyl) surfactants, whose molecular structures are shown schematically in Figure 1. UV–visible absorption spectra (Figure S5, SI) of the cys-less and E50Q PR mutants solubilized exclusively in these surfactants show characteristic absorption properties of functionally active PR, suggesting that these surfactants solubilize functional PR species. Both DDM and Brij-35 have identical 12-carbon alkyl tails but different head groups, namely, a maltoside head group for DDM and a linear ethylene oxide (EO) chain for Brij-35. Thus, the analysis of PR solubilized in DDM versus Brij-35 allows the effects of a

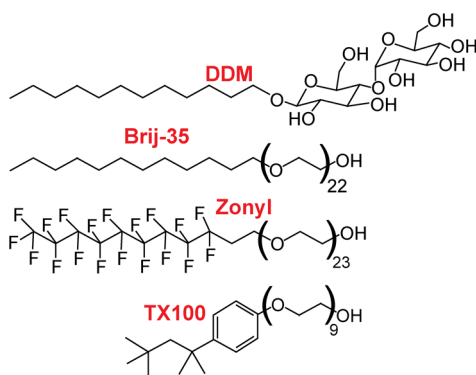


Figure 1. Molecular structures of *n*-dodecyl- β -D-maltoside (DDM), Brij-35, Zonyl FSN-100 (Zonyl), and Triton X-100 (TX100).

surfactant head group type to be probed. In contrast, Triton X-100 (TX100) and Zonyl FSN-100 (Zonyl) surfactants have the same linear ethylene oxide (EO) head groups, albeit with different EO chain lengths as Brij-35, yet dramatically different octylphenolic and linear fluorinated tails, respectively. These surfactants permit the effects of the tail group type on PR function to be assessed.

Quantifying Surfactant Compositions of Micellar Solutions Containing PR. To establish how surfactants influence PR function, it is necessary to understand the surfactant composition in the micellar solution in which PR is solubilized. Solution-state ^1H NMR is a useful method for quantifying the surfactant compositions of MP-solubilizing micellar solutions, yet it is not routinely used.⁴⁰ For example, the single-pulse ^1H NMR spectrum in Figure 2a of 2 mM DDM in D_2O shows peaks at 0.8, 1.3, 1.6, 3.5–4, 4.4, and 5.4 ppm that are unambiguously assigned to the various ^1H moieties of the alkyl tail and maltoside head group of DDM, as indicated in the inset. The integrated areas of these assigned

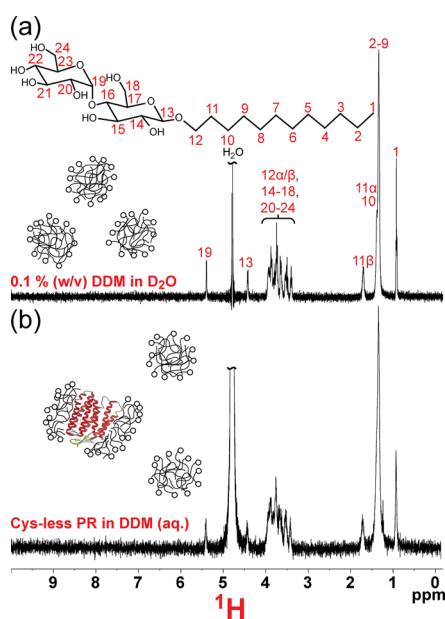


Figure 2. Solution-state ^1H NMR spectra of (a) 2 mM DDM in D_2O and (b) monomeric fractions of cys-less PR from SEC, diluted 20 times in D_2O . A comparison of the respective peak areas among these spectra establishes the DDM concentration in the PR-containing solutions.

^1H signals represent the correct stoichiometry of the ^1H species of a DDM molecule, corroborating their assignments. The ^1H NMR spectrum shown in Figure 2b of cysteine-less (cys-less) PR in a micellar DDM solution shows the same ^1H NMR signals, indicating that DDM is the only surfactant present in this solution. Notably, signals associated with PR molecules are entirely absent in the spectrum shown in Figure 2b, likely because the PR species are too dilute ($\sim 10\ \mu\text{M}$) to be detected or undergo slow motions that reduce NMR spectral resolution. A comparison of these ^1H NMR signals to those from a 2 mM DDM solution, which serves as a quantitative external reference (Figure S6, SI), reveals that this PR sample contains 17.6 mM DDM. Interestingly, the experimentally determined DDM concentration is substantially higher than the 1 mM DDM of the buffer used to purify this very protein sample, suggesting that DDM surfactants accumulate around PR during purification, likely due to the favorable association of surfactants with PR and/or centrifugal concentration. The ^1H NMR spectra recorded from Triton X-100 (TX100), Brij-35, and Zonyl FSN-100 (Zonyl) surfactants in D_2O solutions also show distinct sets of ^1H signals (Figure S7, SI), enabling ^1H NMR analyses to quantify these surfactants in D_2O as well.

Enriching PR Monomer and Oligomer Contents in Micellar Solutions. Comparisons of the functionalities of monomeric and oligomeric PR in different surfactant environments provide important insights into how local surfactant environment and oligomerization influence PR function. However, preparing such samples is often challenging because the monomer/oligomer distributions of PR are often surfactant dependent. We exploit solution-state ^1H NMR spectroscopy and blue-native polyacrylamide gel electrophoresis (BN-PAGE) techniques to obtain a semiquantitative measure for the populations of soluble PR monomers and oligomers.⁴¹ This information can then be used to correlate monomer and oligomer contents with surfactant compositions and the functional properties of PR. The understanding gained from this analysis can be employed to select surfactant compositions or other modifications to isolate predominantly monomeric or oligomeric PR in the same surfactant environment.

Separation of PR Species with Size-Exclusion Chromatography (SEC). Samples enriched in either monomeric or oligomeric PR but with the same surfactant can be prepared by size-exclusion chromatography, demonstrated here for PR in micellar DDM solutions. A BN-PAGE gel run with cys-less PR (Figure 3a, lane 1) that, according to solution-state ^1H NMR, is solubilized in a solution containing 8 mM DDM yields an intense band at $\sim 242\ \text{kDa}$ that is assignable to pentameric/hexameric PR assemblies.²³ The band corresponds to a significantly higher molecular mass than six times the molecular weight of an individual PR molecule (ca. 27 kDa), as would be expected for a PR hexamer. This difference likely arises from the presence of surfactants that are strongly bound to hexameric PR and remain so during the BN-PAGE measurement. As described previously by Hussain et al.,¹⁵ incubation of this pentameric/hexameric cys-less PR sample in concentrated solutions of $\sim 40\ \text{mM}$ diheptanoyl-*sn*-glycero-3-phosphotidylcholine (diC_7PC) surfactants enriches the monomer PR population, which can be subsequently isolated in an SEC column equilibrated with a running buffer of 1 mM DDM without diC_7PC . The resulting monomeric PR fractions obtained from SEC are solubilized in a $\sim 49\ \text{mM}$ DDM solution according to ^1H NMR, whereas the BN-PAGE

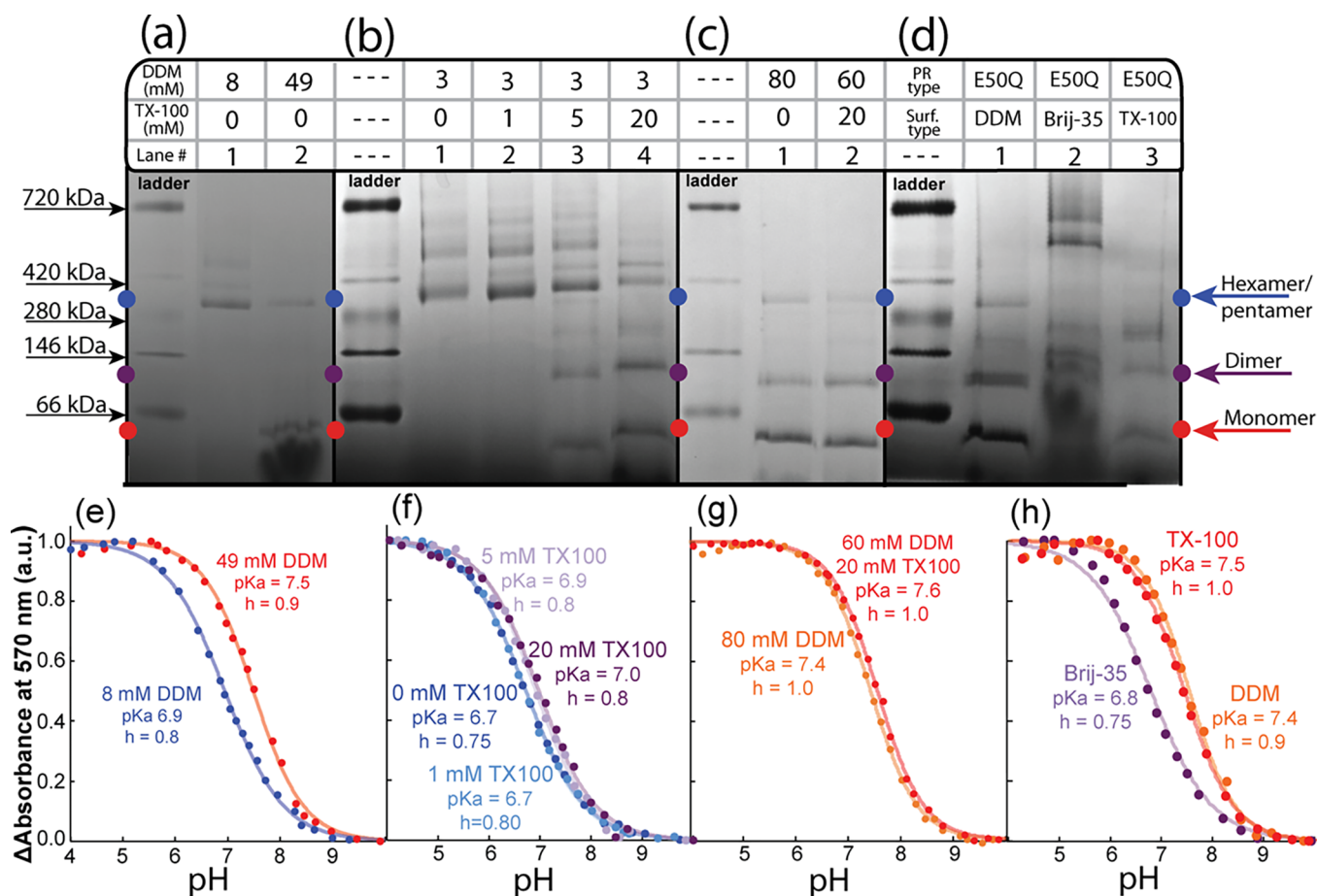


Figure 3. (a–d) Surfactant compositions and blue-native PAGE gels with (e–h) corresponding $pK_{a,PR}$ titration results. The PR samples analyzed in (a) and (e) were solubilized exclusively in DDM surfactants but have distinct monomer and oligomeric distributions. Proteorhodopsin species in samples (b) and (f) were solubilized in low concentrations of DDM but with various TX100 concentrations. In (c) and (g), PR was solubilized in the same total quantity of surfactants but with different DDM and TX100 compositions. Finally, the E50Q PR in (d) and (h) is solubilized exclusively in either DDM, Brij-35, or TX100 surfactants. Samples in (b, c, f, g) were incubated at 4 °C in surfactant solutions for overnight before conducting BN-PAGE and $pK_{a,PR}$ titration measurements.

analysis (Figure 3a, lane 2) showed a strong signal at ~60 kDa that corresponds to monomeric PR²³ and a relatively weak band at ~242 kDa that corresponds to a residual pentamer/hexamer population. The BN-PAGE signal assigned to monomeric PR occurs at a higher molecular weight than expected for a PR molecule (ca. 27 kDa) as well, likely reflecting bound surfactant. Interestingly, the solution-state ¹H NMR spectrum of this predominantly monomeric sample shows no ¹H signals that are assignable to diC₇PC (a ¹H NMR spectrum of neat diC₇PC in D₂O is shown in Figure S7c, SI), suggesting that diC₇PC surfactants elute separately from the PR monomers during SEC. These results demonstrate SEC to be a valuable tool for isolating monomeric and oligomeric PR in the same surfactant type, which enables the examination of the effect of oligomerization on PR function, independent of the surfactant environment.

Tuning the Surfactant Environment of PR Monomers and Oligomers. The populations of monomeric or oligomeric PR can be largely maintained in micellar solutions of various surfactant compositions by judiciously selecting the surfactant concentration and type. For example, monomeric PR should be stable in micellar solutions with surfactants that promote the formation of monomeric PR. Therefore, we sought to identify how DDM, TX100, Brij-35, and Zonyl

surfactants influence the oligomerization behaviors of PR in micellar solutions. First, we investigated the effects of TX100 surfactants on solutions of oligomeric cys-less PR in 3 mM DDM, which were incubated overnight with TX100 in concentrations ranging from 1 to 20 mM and subsequently characterized by BN-PAGE (Figure 3b). Oligomeric cys-less PR incubated in solutions of 3 mM DDM, without TX100 or with 1 mM TX100, were primarily pentameric/hexameric with some higher-order oligomers observed (Figure 3b, lanes 1 and 2), whereas samples containing TX100 concentrations of 5–20 mM showed increasing populations of monomeric and dimeric PR (Figure 3b, lanes 3 and 4). This establishes a proclivity of PR to form monomers or dimers in the presence of TX100 surfactants, which is further corroborated by the BN-PAGE analyses of cys-less PR, as well as monomer-forming E50Q PR variants in DDM incubated with increasing TX100 concentrations (Figure S8, SI).

Importantly, this understanding can be exploited to prepare micellar solutions with similar distributions of PR monomers and oligomers but different surfactant compositions. For example, leveraging the monomer/dimer-forming proclivities of TX100, we incubated monomeric cys-less PR in DDM (obtained from SEC) in solutions containing either 60 mM DDM and 20 mM TX100 or 80 mM DDM. BN-PAGE

analyses of these samples (Figure 3c, lanes 1 and 2) showed nearly identical signal patterns that indicate high populations of monomers with lower quantities of larger oligomers. These results demonstrate that the monomer/oligomer distributions of PR in monomeric PR in DDM micellar solutions can be largely preserved, even in the presence of TX100 surfactants.

Similar analyses conducted on PR in DDM, Brij-35, and Zonyl surfactants revealed how these surfactants influence PR oligomerization. BN-PAGE analyses of cys-less PR incubated in solutions of either DDM or DDM/Brij-35 mixtures (Figure S9, SI) showed that these surfactants solubilize PR as pentamers and hexamers. A BN-PAGE run with PR incubated in solutions containing DDM/Zonyl surfactant mixtures indicated that Zonyl surfactants solubilize PR aggregates that were not visible on BN-PAGE gels (Figure S10a, SI). Complementary UV–visible absorption spectra (Figure S10b, SI) of these same samples revealed increased light scattering with greater Zonyl contents, reflecting the presence of insoluble aggregates that likely form based on an inability of mixtures of Zonyl and DDM surfactants to solubilize PR. The complex behaviors of PR in Zonyl surfactants evade simple analyses by BN-PAGE and, therefore, direct correlations of BN-PAGE and functional data using Zonyl surfactants are excluded in subsequent analyses. Collectively, the BN-PAGE analyses of PR in these diverse surfactant environments underscore the complexities of interactions among surfactants and PR. Still, these data empirically reveal that DDM and Brij-35 surfactants solubilize oligomeric PR, whereas TX100 favors the formation of PR monomers. This dependence can be exploited to correlate surfactant composition with PR function and oligomerization.

Adjusting PR Oligomerization Behaviors by Point Mutations. Point mutations that alter the oligomerization behavior, but not directly the function, of PR provide another important tool to understand the effects of oligomerization on PR function. In this case, the mutated variant and the cys-less protein could display different monomer and oligomer distributions in identical surfactant environments so that differences in protein function could be attributed to effects from oligomerization. Recently, Maciejko et al.²³ used advanced solid-state NMR techniques to identify several residues at the oligomeric interface that mediate PR oligomerization. These mutations included the R51A and D52N mutations that promote the formation of hexameric versus pentameric PR, as well as the E50Q mutation that enriches the population of monomeric PR in DDM and TX100 surfactants. Of specific interest is the monomer-enriching E50Q variant, as this mutant promotes higher monomer populations versus the cys-less protein in a given surfactant environment. To test this, we separately exchanged E50Q and cys-less PR from micellar DDM solutions into new micellar solutions containing exclusively TX100, Brij-35, Zonyl, or DDM (as a control) surfactants and compared their monomer/oligomer distributions by BN-PAGE. Importantly, E50Q PR exchanged into Brij-35, Zonyl, and DDM surfactants retained native-like coloration of functional PR; E50Q PR exchanged into TX100 surfactants had similar native coloration initially, although over several hours turned yellow, signifying the occurrence of structural changes near the retinal chromophore. The BN-PAGE results (Figure 3d) for E50Q PR, when exchanged into different surfactant environments, showed bands associated with monomers and dimers, as well as weaker bands from higher-order oligomers. The exception

was the Brij-35 surfactant environment (Figure 3d, lane 2), in which the higher-order oligomer bands were found to be still intense, further corroborating the propensity of Brij-35 surfactants to solubilize oligomers. Even though the E50Q mutation alone could not eliminate oligomer formation entirely, each E50Q PR solution exhibited higher monomer/dimer contents compared to cys-less PR when exchanged into the respective surfactants (Figure S11, SI). Thus, comparisons of the monomer-forming E50Q and cys-less PR could effectively establish how oligomerization affects protein function in various surfactant environments.

Protonation Behaviors of D97 in Different Surfactant Environments. The protonation behavior of the aspartic acid residue 97 ($pK_{a,D97}$) is a key function-mediating property of PR that provides a sensitive measure for how surfactants and oligomerization influence protein function. Under alkaline conditions, the anionic carboxylic acid moiety of the D97 side chain serves as the primary proton acceptor for the Schiff base⁴² and is crucial for mediating light-activated proton transport by PR.⁴³ As D97 is located near the retinal chromophore, changes in the protonation state of D97 produce a substantial ~ 25 nm shift in the visible absorbance of the retinal, from ~ 515 nm when D97 is deprotonated to ~ 540 nm when D97 is protonated.⁴² This wavelength shift can be equivalently expressed as the difference absorbance at 570 nm (ΔA_{570}), which is the difference in absorbance intensity at 570 nm between PR at a pH of interest and PR under alkaline (\sim pH 10) conditions at which D97 is fully deprotonated. For example, as shown in Figure 3e for primarily monomeric cys-less PR (solubilized in 49 mM DDM, the same sample analyzed in Figure 3a, lane 2), ΔA_{570} decreased sigmoidally from 1.0 under acidic pH conditions to 0.0 at basic pH (Figure 3e, red dots). A fit of these data to the Henderson–Hasselbalch equation (Figure 3e, red line) yielded a $pK_{a,D97}$ of 7.5 and a Hill coefficient of 0.9, reflecting slightly anticooperative protonation of D97 residues in this predominantly monomeric sample. By comparison, pentameric/hexameric PR in 8 mM DDM (same sample as analyzed in Figure 3a, lane 1) exhibited a substantially lower $pK_{a,D97}$ of 6.9 and a moderately reduced Hill coefficient of 0.8 (Figure 3e blue). As only DDM surfactants solubilized PR in both samples, the distinct protonation behaviors are attributable to the differences in monomeric and oligomeric populations. These results imply that the carboxylic moiety of the D97 residues of oligomeric PR is more acidic (i.e., deprotonates at lower pH) and exhibit a slightly more anticooperative protonation than those of monomeric PR.

Examining cys-less PR solubilized in solutions of different TX100 concentrations revealed the influence of TX100 surfactants on the protonation behaviors of D97. Cys-less PR in solution with TX100-to-DDM molar ratios of 0:1 or 1:3 exhibited identical $pK_{a,D97}$ values of 6.7, whereas at ratios of 5:3 or 20:3, the $pK_{a,D97}$ only slightly increased to 6.8 and 7.0, respectively (Figure 3f). These $pK_{a,D97}$ values rose concomitantly with monomer PR content, as established by BN-PAGE (Figure 3b), independent of the presence and concentration of TX100. In other words, TX100 plays a minor role in mediating $pK_{a,D97}$; rather, the TX100-to-DDM molar ratio that varies with the sample preparation method tunes the PR monomer/oligomer content that, in turn, tunes the $pK_{a,D97}$. Comple-

mentary BN-PAGE and pK_{aD97} measurements of E50Q PR variants incubated in solutions with TX100 and DDM also found increased pK_{aD97} values to correlate with greater monomer content (Figure S8, SI). These results are further corroborated by the near-identical D97 protonation behavior of monomeric/dimeric cys-less PR in solutions containing 80 mM surfactant at TX100-to-DDM molar ratios of 0:1 and 1:3 (Figure 3c, lanes 1 and 2), which exhibited pK_{aD97} values of 7.4 and 7.6, respectively, and Hill coefficients of 1.0 (Figure 3g). The slightly (~ 0.2 pH unit) higher pK_{aD97} observed for monomeric PR in 60 mM DDM and 20 mM TX100 can be reconciled with the marginally lower oligomer content in this solution than monomeric PR in 80 mM DDM. Thus, for cys-less PR in solutions with TX100/DDM molar ratios up to ~ 6 , TX100 appears to exert relatively little influence over the pK_a or the Hill coefficient of D97 compared to oligomerization.

Comparisons of the oligomer-destabilizing E50Q variant and cys-less PR in similar surfactant environments revealed additional information about how surfactants and oligomerization mediate D97 protonation. As shown in Figure 3h, E50Q PR in micellar DDM and TX100 solutions showed similar pK_{aD97} values of 7.4 and 7.5, respectively, whereas E50Q PR solubilized in Brij-35 solutions exhibited a lower pK_{aD97} of 6.8 and a Hill coefficient of ~ 0.75 . By comparison, cys-less PR in micellar DDM, TX100, and Brij-35 solutions has pK_{aD97} values of 6.9, 6.8, and 6.6, respectively (Figure S11, SI), i.e., consistently lower pK_{aD97} compared to E50Q PR in the respective surfactant environment. Hence, these data correlate the higher pK_{aD97} values with increased monomer content found in E50Q PR solutions in three separate surfactant environments, clearly establishing oligomerization as a predominant factor in tuning the pK_{aD97} of surfactant-solubilized PR.

Quantitative Correlations of pK_{aD97} and Monomer/Dimer Content. A quantitative correlation of the pK_{aD97} values and BN-PAGE signals provides more direct insight into the relationships between oligomerization, surfactant environments, and the protonation behaviors of D97. Based on the work by Ran et al.,³⁷ we hypothesized that the presence or absence of a W34–H75 interprotein hydrogen bond accounts for the distinct D97 protonation behaviors of monomeric ($pK_{aD97} \sim 7.5$, Hill coeff. ~ 1.0) and oligomeric ($pK_{aD97} \sim 6.9$, Hill coeff. ≤ 0.8) PR. In this case, we assumed that PR trimers or oligomers of higher order could support W34–H75 hydrogen bonding among each PR subunit and consequently yield lower (~ 6.8) pK_{aD97} values; in contrast, monomeric PR and one of the protein subunits of dimeric PR would not support such interprotein W34–H75 hydrogen bonds and, as a consequence, would exhibit higher pK_{aD97} values (~ 7.5). To test this, we correlated the sum of the monomer and 1/2 of the dimer contents, as estimated from the integrated peak areas of the associated BN-PAGE bands, with the pK_{aD97} values of all cys-less and E50Q PR samples examined in this study. The resulting correlation (Figure 4) includes data from 40 different cys-less and E50Q PR samples solubilized in micellar surfactant solutions, constituted of DDM (Figure 4, blue), TX100 (Figure 4, red), or Brij-35 (Figure 4, orange), either exclusively or in mixtures with DDM. A best-fit linear line

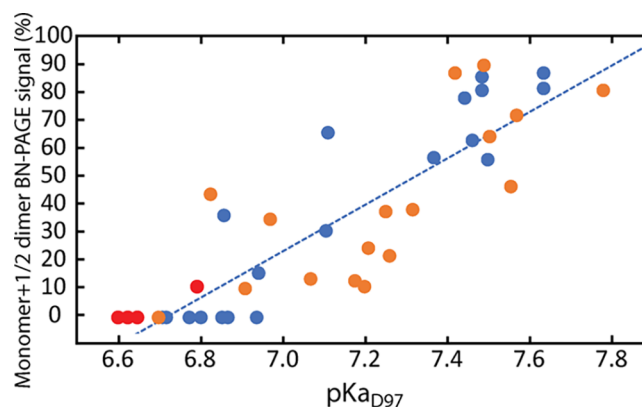


Figure 4. Correlation of pK_{aD97} values and integrated monomer/dimer band intensities from BN-PAGE analyses for WT or E50Q PR in micellar solutions that contained exclusively DDM (blue), TX100 (orange), or Brij-35 (red) surfactants either exclusively or in mixtures with DDM. Monomer/dimer contents were estimated as the sum of the integrated BN-PAGE band intensities associated with the monomers and one-half that of dimers, normalized to the total integrated intensity in the same lane. The dashed blue line is a best fit line to all the data points in this figure that has a Pearson correlation coefficient of 0.87, reflecting a strong correlation of monomer/dimer content with pK_{aD97} values.

(Figure 4, blue dashed) to every data point in Figure 4 yielded a Pearson's correlation coefficient of +0.87 that establishes a strong correlation of pK_{aD97} with monomer/dimer content. Moreover, the data range along the abscissa, which characterizes the effects of oligomerization, is 1.1 pH unit (from 6.6 to 7.7), whereas the average deviation along the ordinate, where surfactant effects manifest, is relatively lower at 0.15 from the best-fit line. This quantitatively supports that oligomerization of surfactant-solubilized PR plays a more significant role in adjusting pK_{aD97} values than the surfactant environment. Interestingly, the Hill coefficient correlated poorly with monomer/dimer contents (see Figure S12), indicating that the cooperativity of D97 protonation is not or insignificantly influenced by oligomerization alone.

The pK_{aD97} dependencies reported here generally agree with the literature on green-absorbing PR in micellar solutions, which typically range from 6.9 to 8.2,^{23,44,45} though higher values were observed when certain anions are present.⁴⁶ Although few studies explored the effects of different surfactants on the pK_{aD97} of PR, Maciejko et al.²³ reported pK_{aD97} values of ~ 6.8 for pentameric PR in DDM and ~ 8.0 for monomeric PR in octylglucoside surfactants, which are consistent with the results presented here. The same study, however, also reported a pK_{aD97} value of ~ 6.8 for monomeric PR in micellar TX100 surfactant solutions, which is much lower than would be expected, should oligomerization predominantly adjust the pK_{aD97} of PR. A possible explanation for this apparent inconsistency could be the method these researchers used to prepare PR in TX100 environments; namely, TX100-solubilized PR was purified by directly extracting PR in *E. coli* membranes using TX100, rather than extracting in DDM and then exchanging into TX100, as conducted in this study. Should the extraction of membrane-embedded PR by TX100 proceed inefficiently or incompletely, the local environment of TX100-solubilized PR could also

include lipid molecules, which could influence the pK_{aD97} . Indeed, lipid composition influences the pK_{aD97} of photoactive PR monomers in phospholipid nanodiscs.⁴⁷ Moreover, our laboratories have also observed that PR in lipid environments generally has low (<7.0) pK_{aD97} values, independent of the oligomeric state (manuscript in preparation). Thus, the presence of lipids could account for the uncharacteristically low pK_{aD97} values for TX100-solubilized PR monomers observed by Maciejko et al.²³ Given this factor and the general agreement of our results with Maciejko et al., it appears likely that the pK_{aD97} for PR in micellar TX100 solutions would concur with our data and analyses, if similar sample preparation protocols were used.

Effect of Oligomerization on PR Photocycle Kinetics.

Motivated by the distinct dependence of the protonation behaviors of D97 on oligomerization, we interrogated how oligomerization influences the proton-pumping kinetics of PR by probing the light-activated responses of monomeric and oligomeric PR in micellar DDM solutions. Following absorption of green light, PR undergoes a cyclic sequence of small- and large-scale motions that result in the net transport of protons from the cytoplasmic to the extracellular side of PR at a turnover rate of approximately ~ 20 ms.⁴² Several of these motions perturb the local environment of the retinal chromophore and alter its absorbance, enabling the proton-pumping kinetics to be analyzed by transient optical absorbance spectroscopy. Predominantly monomeric PR in an alkaline micellar DDM solution, the same sample analyzed in Figure 3a (lane 2), upon activation by a green (532 nm) laser pulse (~ 10 ns) showed complex light absorption behaviors. These are presented in Figure 5a, solid lines, as difference absorbances, i.e., the differences in the absorbance intensity of PR at some time after light activation from that in the nonactivated state, detected prior to light activation. Importantly, even though the transient absorbance responses of pentameric/hexameric PR in 8 mM DDM (Figure 5a, dashed lines), the same sample analyzed in Figure 3a (lane 1), appeared qualitatively similar to those of the monomeric PR, they occur over dramatically different time scales that reflect key functional differences between them that are attributable to oligomerization.

Qualitative insights into the different light-activated kinetic behaviors of PR monomers and oligomers can be obtained by interpreting the absorbance responses in terms of the photochemical reaction cycle model developed by Váró et al. for PR.³⁶ This cyclic sequential reaction model, depicted in Figure 5b, includes five intermediates (K, M₁, M₂, N, and PR') with distinct absorption signatures and lifetimes³⁶ that enable the transient difference absorbances to be associated with the intermediate populations. For difference absorbance data from monomeric PR in Figure 5a (solid lines), a positive intensity arose at 590 nm at early times (~ 10 μ s) after light activation, which can be attributed to the presence of the K intermediate species that absorb maximally at ~ 555 nm. The subsequent decay of this intensity occurred concurrently with a rise in absorbance at ~ 410 nm, which can be attributed exclusively to the M intermediates, signifying a conversion of the K to M₁ intermediate. At times >60 μ s, the absorbance at 410 nm also decayed, whereas the 590 nm absorbance increased, reflecting a rising population of PR molecules in the N intermediate configuration. All intensities decayed to zero by ~ 300 ms, as

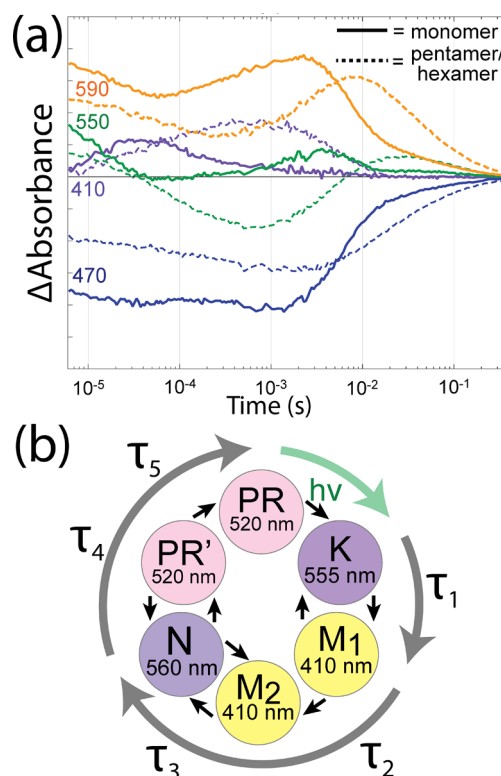


Figure 5. (a) Transient visible absorbance data collected from the same samples that were analyzed in Figure 3a that contain mostly (solid lines) monomeric and (dotted lines) pentameric/hexameric in alkaline (pH 8.5) DDM solutions at ~ 20 °C. Transient absorbance data were also collected at 500, 570, and 630 nm from these same samples, which are shown in Figure S8. (b) Schematic diagram of the photochemical reaction cycle of proteorhodopsin under basic conditions, which includes K, M₁, M₂, N, and PR' intermediates.³⁶

the N and PR' intermediates converted back to the nonactivated PR state.

Distinctions among the difference absorbance signals at 410 and 590 nm, associated with the respective M and K/N intermediates, revealed important photocycle kinetics that are altered by oligomerization. Specifically, the maximum intensity of the 410 nm difference absorbance occurred at a much shorter time (~ 40 μ s) for the predominantly monomeric PR sample, which was prepared using SEC, compared to pentameric/hexameric PR (~ 800 μ s) (Figure 5a, purple solid and dashed lines). Moreover, the ratio of the 410 nm to 590 nm difference absorbance intensities was generally much greater for the pentameric/hexameric PR than for the monomeric PR population. These observations establish that M₁ and/or M₂ intermediates of pentameric/hexameric PR accumulate at later times and in greater quantities, versus in monomeric PR. For bacteriorhodopsin (BR), monomers accumulate more rapidly in the M intermediate state as compared to oligomers,^{48,49} similar to the photocycle kinetic properties found for PR monomers compared to oligomers. This trend is possibly due to greater flexibility in the secondary structure of BR and PR monomers relative to their oligomeric counterparts that could be constrained by close interactions and proximities of neighboring protomers. Greater flexibility in the secondary and tertiary protein structures could facilitate structural changes that are associated with transitions between photocycle intermediates, which occur for PR and BR.^{53,54} The

difference absorbance at 590 nm also passed through a maximum value at significantly delayed times for pentameric/hexameric PR (~ 8 ms) versus monomeric PR (2–3 ms) (Figure 5a, orange solid and dashed lines), revealing that PR oligomers accumulate in the N intermediate configuration at later times.

A global fitting analysis, as used previously by Dioumaev et al.,⁴² of the transient difference absorbance data in Figure 5a provided a more quantitative comparison of the photochemical reaction kinetics for PR monomers and PR oligomers. Such an analysis fits the difference absorbance intensities at each wavelength with a sum of monoexponential decays, with wavelength-dependent pre-exponential factors and mutual (wavelength-independent) exponential time constants. Global fit analyses were performed on difference absorbance data collected from predominantly monomeric (same sample analyzed in Figure 3a, lane 1) or oligomeric (same sample analyzed in Figure 3b, lane 2) cys-less PR at seven different wavelengths, the four wavelengths shown in Figure 5a along with those at 470, 550, and 630 nm. Plots of the transient difference absorbances at all seven wavelengths for each sample are shown in Figure S8. Global fit analyses were performed with three to six exponential terms; the sum of squared residuals for each fit decreased significantly up to the use of five kinetic exponential terms, above which little improvement was observed (Figure S13). Therefore, we compare global fits obtained using five exponential terms for both monomeric and oligomeric PR (Figure S14, SI). The five time constants from the five-exponential global fit are shown in Table 1 and reflect the apparent time scales for interconversions among two or more intermediates. Using as a guide the analyses by Varó et al. for PR in *E. coli* lipids,³⁶ the τ_1 constant largely characterizes the decay of the K and rise of the M intermediates, whereas τ_2 and τ_3 are associated with a decrease in the populations of M and rise in N intermediates, as well as the equilibria among the M_2 and N intermediates, as shown schematically in Figure 5b. The time constants τ_4 and τ_5 reflect the interconversions among the N and PR' intermediates and the nonactivated PR state, respectively. Our analysis found that the time constants τ_1 – τ_4 are 2–3 times shorter for monomeric compared to pentameric/hexameric PR, indicating that the early steps of the photocycle are 2–3 times faster for PR monomers. Transient difference absorbance measurements recorded from oligomeric PR in solutions at different DDM concentrations (Figure S9) showed nearly identical absorbance behaviors, suggesting little to no influence of DDM concentrations on the PR photocycle. These analyses underscore the substantial dependence of the photocycle kinetics of PR on oligomerization.

Photocycle Kinetics of PR on Different Surfactants.

The characteristic photocycle kinetics of monomeric and oligomeric cys-less PR in DDM surfactants provides us with an experimental handle to analyze the influence of surfactant

environments on the photocycle kinetics of PR, here illustrated for E50Q PR in DDM, Brij-35, TX100, and Zonyl surfactant environments. For example, for primarily monomeric E50Q PR in DDM, the 410 and 590 nm difference absorbances (Figure 6a) exhibited maxima at $\sim 4 \times 10^{-5}$ and 2×10^{-3} s, respectively, which align precisely with those of monomeric cys-less PR in 49 mM DDM (Figure 5a). By comparison, the difference absorbances at 410 and 590 nm of E50Q PR in Brij-35 (Figure 6b), which has lower monomer content, exhibited maxima at significantly later times ($\sim 2 \times 10^{-4}$ and $\sim 1 \times 10^{-3}$ s, respectively), which closely agree with those of pentameric/hexameric cys-less PR in DDM ($\sim 6 \times 10^{-4}$ and $\sim 8 \times 10^{-3}$ s, Figure 5a). Thus, the effect of oligomerization alone can reconcile the absorbance behaviors of E50Q PR in both micellar DDM and Brij-35 solutions, further establishing that DDM and Brij-35 surfactant environments do not distinctly influence PR function. Corroborating this conclusion are the light-activated transient absorbances (Figure S9, SI) of cys-less PR incubated in DDM or DDM/Brij-35 mixtures, which again correlate longer photocycle time scales with greater oligomer contents. Oligomerization can also explain some of the absorbance behaviors of E50Q PR in TX100 and Zonyl FSN-100 surfactant environments. In particular, the 410 nm difference absorbance passes through a maximum at early times (4×10^{-5} s) for highly monomeric E50Q in a TX100 solution (Figure 6c) and at later times (1×10^{-3} s) for E50Q in a Zonyl surfactant solution (Figure 6d), consistent with the latter being predominantly oligomeric PR, as would be anticipated based on its low pK_{aD97} value (~ 6.6). Overall, these analyses demonstrate oligomerization to be a general

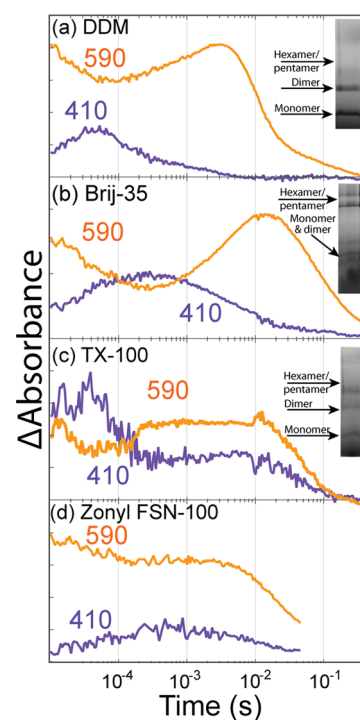


Figure 6. Transient visible absorbance differences of surfactant-solubilized E50Q PR exchanged from DDM into (a) DDM, (b) Brij-35, and (c) TX100 surfactants. The E50Q PR samples exchanged into DDM and TX100 surfactants showed a distribution of monomers and dimers, whereas E50Q PR in Brij-35 surfactants was primarily oligomeric. Measurements were conducted at pH ~ 8.5 .

Table 1. Apparent Time Constants for the Photochemical Reaction Cycle of Monomeric or Oligomeric Proteorhodopsin in Micellar DDM Solutions^a

	τ_1 (μ s)	τ_2 (μ s)	τ_3 (ms)	τ_4 (ms)	τ_5 (ms)
monomer (49 mM DDM)	13	130	1.6	5.2	89
oligomer (8 mM DDM)	47	380	3.9	14	103

^aThe time-constant values were obtained from global fitting analyses of the time-resolved UV–visible absorbance data in Figure 5a.

means to modify PR function among DDM, Brij-35, TX100, and Zonyl surfactant environments.

However, E50Q PR in TX100 and Zonyl micellar solutions also exhibits subtle absorbance characteristics that cannot be solely explained by oligomerization. For example, for E50Q PR in TX100, the difference absorbance at 410 nm, which is associated with the M intermediates, yielded a local maximum at $\sim 7 \times 10^{-3}$ s, which is a greater delay than observed for any monomeric or oligomeric PR solution studied here. Thus, this feature is attributed to the TX100 surfactant environment that appears to promote the slower accumulation of M intermediates. Separately, for E50Q PR in Zonyl surfactants (Figure 6d), the 410 nm difference absorbance also exhibited a maximum at relatively late times ($\sim 9 \times 10^{-4}$ s) which is characteristic of oligomeric cys-less PR in DDM; however, the 590 nm difference absorbance reaches a maximum at $\sim 3 \times 10^{-3}$ s, as observed for monomeric cys-less PR in DDM (Figure 5a). Therefore, E50Q PR in Zonyl surfactant environments exhibits characteristics associated with both monomeric and oligomeric PR, indicating that the Zonyl surfactants influence PR function. These analyses clearly establish that surfactant environment can modify PR function, as reflected in the alteration of the photocycle kinetics.

The photocycle and BN-PAGE analyses were used together to correlate subtle changes in the photocycle kinetics of PR with different surfactant species in micellar solutions. With reference to the photocycle kinetics of DDM-solubilized PR, Brij-35 surfactant environments exerted little influence over the PR photocycle, whereas both TX100 and Zonyl surfactants imparted minor and distinct effects on the photocycle kinetics. These trends in photocycle behavior correlate with the structure of the surfactant tail: both DDM and Brij-35 have identical dodecylalkyl tails, whereas TX100 and Zonyl surfactants have dramatically different alkyl-phenyl and linear fluorinated alkyl tails, respectively. By comparison, DDM and Brij-35 have distinct maltoside and ethylene oxide head groups, respectively, but do not promote different photocycle behaviors, suggesting a lesser role of the hydrophilic surfactant head groups in mediating PR function. This is borne out by the distinct effects of Zonyl and TX100 surfactants on the PR photocycle, despite the similar ethylene oxide head groups of these surfactants. Therefore, surfactant effects observed here appear to originate from the surfactant tail moieties, rather than the head groups.

The results also reveal clear trends of PR function with oligomerization and surfactant environment in micellar surfactant solutions, which motivate the study of PR function in more native lipid environments. Although micellar surfactant environments support the native-like structure and function of PR, such environments are distinct from native lipid bilayers of marine bacteria in which PR naturally resides. This begs the question whether the functional trends with oligomerization and surfactant environment observed here for PR in micellar surfactant environments translate to PR in different lipid environments. The two measures of PR function examined here were the $pK_{a,D97}$ value associated with the important D97 aspartic acid residue, which reflects the pH-dependent equilibria of the alkaline and acidic states of PR, and the light-activated photocycle kinetics, which is associated with nonequilibrium conformational motions and protonation/deprotonations that mediate proton transport. Ongoing (unpublished) studies of PR reconstituted in liposomes show

that the differences in light-activated photocycle kinetics observed for surfactant-solubilized PR monomers and oligomers hold in the lipid environment but that the $pK_{a,D97}$ value is dictated by the lipid environment.⁵⁰ The structural and mechanistic basis of function tuning by oligomerization and the environment of PR remains an important issue. This study establishes that PR oligomerization influences PR function in surfactant environments, which is expected to motivate future studies, especially as functional tuning by oligomerization is likely not a unique property of PR.

Although this study focused on PR, it is interesting to consider whether oligomerization tunes the functionalities of other transmembrane proteins, which would reflect the general physiological importance of membrane protein oligomerization. There are several studies on the functional effects of other oligomer-forming light-activated transmembrane proteins, such as bacteriorhodopsin (BR) and rhodopsin (Rho). Under specific conditions, both BR and Rho can organize as either monomers or oligomers.^{17,48,49,51,52} Interestingly, the effect of oligomerization on BR and Rho function varies. For BR, monomers and oligomers exhibit similar proton-pumping rates and photocycle kinetics at early picosecond time scales;^{48,49,52} yet, the photocycle kinetics of BR at later times is markedly different, with monomeric BR accumulating in the "M" intermediate state more rapidly than oligomers.^{48,49} These behaviors mirror our observations that PR monomers accumulate more rapidly in the M state than oligomeric PR, potentially reflecting a homologous mechanism by which oligomerization tunes PR and BR function. Interestingly, however, Rho monomers and oligomers show nearly identical photocycle kinetics,¹⁷ so oligomerization does not appear to be a universal mechanism to modify seven-helical transmembrane protein function.

Although only a limited number of studies interrogate the role of surfactants in BR function, their observations are mostly consistent with those of our studies of PR. The functional behaviors of BR monomers are comparable in different nonionic surfactants, such as Triton X-100 and octylglucoside surfactants,⁴⁹ whereas ionic surfactants clearly influence the photocycle kinetics of oligomeric BR, in particular the deprotonation/reprotonation rates of the Schiff base.⁵⁵ We also observed that nonionic DDM and Brij-35 promoted similar photocycle behaviors for PR, yet TX100 and Zonyl surfactants modulated the photocycle kinetics of PR, albeit much more subtly versus the effects of oligomerization. Differences in the effects of TX100 on PR and BR function are especially interesting, considering that TX100 promotes monomer formation for both proteins. As TX100 appeared to delay the formation of the M intermediate in PR but not in BR, we speculate that TX100 interacts more strongly with PR than with BR and thus constrains the conformational changes required for PR to undergo the photochemical reaction cycle. In other words, oligomerization is a dominant, but not the exclusive, modulator of PR function.

CONCLUSIONS

The influences of oligomerization and local surfactant environments on the functionality of the transmembrane protein proteorhodopsin (PR) solubilized in micellar surfactant solutions have been studied. The combined use of solution-state ¹H NMR and blue-native PAGE techniques enabled the systematic correlation of surfactant compositions,

PR oligomerization behaviors, and PR function, as measured by the protonation behaviors of the D97 residue and photocycle kinetics associated with proton transport. The pK_a for the aspartic acid residue D97 ($pK_{a,D97}$) was uniformly higher for monomeric PR ($pK_{a,D97}$ 7.5–7.7) than for oligomeric PR ($pK_{a,D97} \sim 6.6$ –6.9), regardless of the concentration and type of solubilizing surfactant, which in this study included DDM, TX100, and Brij-35. Under alkaline conditions (pH \sim 8.5), the photocycle kinetics at early times was 2–3 times faster for PR monomers, compared to oligomeric PR in DDM-containing micellar solution. Detailed analyses of cys-less PR and the monomer-forming E50Q variant corroborated that these differences persisted in different DDM, Brij-35, TX100, and Zonyl surfactant environments, demonstrating oligomerization to be a dominant mechanism by which surfactant-constituted PR adjusts function. Still, in few cases, the light-activated kinetics of PR was subtly modified by the surfactant environment, which correlated with the molecular structure of the surfactant tail. However, whether and how oligomerization of lipid-constituted PR adjusts protein function is an open question. Although the analyses here focused on PR, these findings are expected to apply more broadly to other transmembrane protein oligomers that have important physiological or therapeutic roles.

■ ASSOCIATED CONTENT

■ Supporting Information

The Supporting Information is available free of charge on the ACS Publications website at DOI: 10.1021/acs.jpcc.9b00922.

Solution ^1H NMR spectra recorded from solutions of E50Q PR in TX100, Brij-35, and DDM surfactants (Figure S1); BN-PAGE integration procedure (Figure S2); BN-PAGE results of cys-less PR under various pH conditions and before and after pH titrations used to measure the pK_a of D97 (Figure S3); three pK_a curves acquired from three cys-less PR samples prepared identically (Figure S4); UV–visible absorbance properties of PR in DDM, TX100, Brij-35, and Zonyl surfactant environments (Figure S5); ^1H NMR spectra of the different micellar surfactants studied at various concentrations (Figures S6 and S7); BN-PAGE results and either the $pK_{a,D97}$ values, transient absorbances or static UV–visible absorbances acquired from PR in different micellar surfactant solutions (Figure S8–S11); plot of Hill coefficient versus monomer plus 1/2 dimer content for PR solubilized in various surfactant solutions (Figure S12); global fitting analyses performed using various time constants on time-resolved absorption data from predominantly monomeric and oligomeric PR (Figures S13 and S14); PR concentrations, surfactant concentrations, and pH conditions used for various measurements in this study (Table S1); MATLAB codes used to analyze UV-visible absorbance data (PDF)

■ AUTHOR INFORMATION

Corresponding Author

*E-mail: songi@chem.ucsb.edu. Tel: (805) 893-4858.

ORCID

Matthew N. Idso: 0000-0001-5685-0870

Bradley F. Chmelka: 0000-0002-4450-6949

Songi Han: 0000-0001-6489-6246

Notes

The authors declare no competing financial interest.

■ ACKNOWLEDGMENTS

The authors thank Dr. L. Laverman for help with the transient optical absorbance experiments and Drs. J. Lanyi and S. Balashov for helpful discussions concerning the difference absorbance analyses. This work was supported by the Institute for Collaborative Biotechnologies through grant W911NF-09-0001 from the U.S. Army Research Office and the National Institutes of Health R01GM116128. The content of the information does not necessarily reflect the position or the policy of the U.S. government, and no official endorsement should be inferred. Solution NMR measurements were conducted using instrumentation in the MRL Shared Experimental Facilities at the University of California, Santa Barbara. The MRL Shared Experimental Facilities are supported by the MRSEC Program of the NSF under Award No. DMR 1720256, a member of the NSF-funded Materials Research Facility Network.

■ REFERENCES

- (1) Yan, N. A Glimpse of Membrane Transport through Structures—Advances in the Structural Biology of the GLUT Glucose Transporters. *J. Mol. Biol.* **2017**, *429*, 2710–2725.
- (2) Berndt, A.; Lee, S. Y.; Wietek, J.; Ramakrishnan, C.; Steinberg, E. E.; Rashid, A. J.; Kim, H.; Park, S.; Santoro, A.; Frankland, P. W.; et al. Structural Foundations of Optogenetics: Determinants of Channelrhodopsin Ion Selectivity. *Proc. Natl. Acad. Sci. U.S.A.* **2016**, *113*, 822–829.
- (3) Wang, J.; Albers, T.; Grewer, C. Energy Landscape of the Substrate Translocation Equilibrium of Plasma-Membrane Glutamate Transporters. *J. Phys. Chem. B* **2018**, *122*, 28–39.
- (4) Bragin, P. E.; Mineev, K. S.; Bocharova, O. V.; Volynsky, P. E.; Bocharov, E. V.; Arseniev, A. S. HER2 Transmembrane Domain Dimerization Coupled with Self-Association of Membrane-Embedded Cytoplasmic Juxtamembrane Regions. *J. Mol. Biol.* **2016**, *428*, 52–61.
- (5) Kaplan, J. H. Biochemistry of Na,K-ATPase. *Annu. Rev. Biochem.* **2002**, *71*, 511–535.
- (6) Lefkowitz, R. J. Historical Review: A Brief History and Personal Retrospective of Seven-Transmembrane Receptors. *Trends Pharmacol. Sci.* **2004**, *25*, 413–422.
- (7) Rampelt, H.; Bohnert, M.; Zerbes, R. M.; Horvath, S. E.; Warscheid, B.; Pfanner, N.; van der Laan, M. Mic10, a Core Subunit of the Mitochondrial Contact Site and Cristae Organizing System, Interacts with the Dimeric F1Fo-ATP Synthase. *J. Mol. Biol.* **2017**, *429*, 1162–1170.
- (8) Ferré, S.; Casadó, V.; Devi, L. A.; Filizola, M.; Jockers, R.; Lohse, M. J.; Milligan, G.; Pin, J.-P.; Guitart, X. G Protein-Coupled Receptor Oligomerization Revisited: Functional and Pharmacological Perspectives. *Pharmacol. Rev.* **2014**, *66*, 413–434.
- (9) Klyszejko, A. L.; Shastri, S.; Mari, S. A.; Grubmüller, H.; Müller, D. J.; Glaubitz, C. Folding and Assembly of Proteorhodopsin. *J. Mol. Biol.* **2008**, *376*, 35–41.
- (10) Stone, K. M.; Voska, J.; Kinnebrew, M.; Pavlova, A.; Junk, M. J. N.; Han, S. Structural Insight into Proteorhodopsin Oligomers. *Biophys. J.* **2013**, *104*, 472–481.
- (11) Schonenbach, N. S.; Rieth, M. D.; Han, S.; O'Malley, M. A. Adenosine A2a Receptors Form Distinct Oligomers in Protein Detergent Complexes. *FEBS Lett.* **2016**, *590*, 3295–3306.
- (12) Jastrzebska, B.; Maeda, T.; Zhu, L.; Fotiadis, D.; Filipek, S.; Engel, A.; Stenkamp, R. E.; Palczewski, K. Functional Characterization of Rhodopsin Monomers and Dimers in Detergents. *J. Biol. Chem.* **2004**, *279*, 54663–54675.

- (13) Rietveld, A. W. M.; Ferreira, S. T. Kinetics and Energetics of Subunit Dissociation/Unfolding of TIM: The Importance of Oligomerization for Conformational Persistence and Chemical Stability of Proteins. *Biochemistry* **1998**, *37*, 933–937.
- (14) Burnett, B. G.; Muñoz, E.; Tandon, A.; Kwon, D. Y.; Sumner, C. J.; Fischbeck, K. H. Regulation of SMN Protein Stability. *Mol. Cell. Biol.* **2009**, *29*, 1107–1115.
- (15) Hussain, S.; Kinnebrew, M.; Schonenbach, N. S.; Aye, E.; Han, S. Functional Consequences of the Oligomeric Assembly of Proteorhodopsin. *J. Mol. Biol.* **2015**, *427*, 1278–1290.
- (16) Schonenbach, N. S.; Hussain, S.; O'Malley, M. A. Structure and Function of G Protein-Coupled Receptor Oligomers: Implications for Drug Discovery. *Wiley Interdiscip. Rev.: Nanomed. Nanobiotechnol.* **2015**, *7*, 408–427.
- (17) Tsukamoto, T.; Demura, M.; Sudo, Y. Irreversible Trimer to Monomer Transition of Thermophilic Rhodopsin upon Thermal Stimulation. *J. Phys. Chem. B* **2014**, *118*, 12383–12394.
- (18) Veenhoff, L. M.; Heuberger, E. H. M. L.; Poolman, B. Quaternary Structure and Function of Transport Proteins. *Trends Biochem. Sci.* **2002**, *27*, 242–249.
- (19) Veatch, W.; Stryer, L. The Dimeric Nature of the Gramicidin A Transmembrane Channel: Conductance and Fluorescence Energy Transfer Studies of Hybrid Channels. *J. Mol. Biol.* **1977**, *113*, 89–102.
- (20) Chitnis, P. R. Photosystem I: Function and Physiology. *Annu. Rev. Plant Physiol. Plant Mol. Biol.* **2001**, *52*, 593–626.
- (21) Wang, S.; Munro, R. A.; Kim, S. Y.; Jung, K.-H.; Brown, L. S.; Ladizhansky, V. Paramagnetic Relaxation Enhancement Reveals Oligomerization Interface of a Membrane Protein. *J. Am. Chem. Soc.* **2012**, *134*, 16995–16998.
- (22) Milikisiyants, S.; Wang, S.; Munro, R. A.; Donohue, M.; Ward, M. E.; Bolton, D.; Brown, L. S.; Smirnova, T. I.; Ladizhansky, V.; Smirnov, A. I. Oligomeric Structure of Anabaena Sensory Rhodopsin in a Lipid Bilayer Environment by Combining Solid-State NMR and Long-Range DEER Constraints. *J. Mol. Biol.* **2017**, *429*, 1903–1920.
- (23) Maciejko, J.; Mehler, M.; Kaur, J.; Lieblein, T.; Morgner, N.; Ouari, O.; Tordo, P.; Becker-Baldus, J.; Glaubitz, C. Visualizing Specific Cross-Protomer Interactions in the Homo-Oligomeric Membrane Protein Proteorhodopsin by DNP-Enhanced Solid-State NMR. *J. Am. Chem. Soc.* **2015**, *137*, 9032–9043.
- (24) Chawla, U.; Jiang, Y.; Zheng, W.; Kuang, L.; Perera, S. M. D. C.; Pitman, M. C.; Brown, M. F.; Liang, H. A Usual G-Protein-Coupled Receptor in Unusual Membranes. *Angew. Chem.* **2016**, *128*, 598–602.
- (25) Rosevear, P.; VanAken, T.; Baxter, J.; Ferguson-Miller, S. Alkyl Glycoside Detergents: A Simpler Synthesis and Their Effects on Kinetic and Physical Properties of Cytochrome c Oxidase. *Biochemistry* **1980**, *19*, 4108–4115.
- (26) Lund, S.; Orłowski, S.; de Foresta, B.; Champeil, P.; le Maire, M.; Möller, J. V. Detergent Structure and Associated Lipid as Determinants in the Stabilization of Solubilized Ca²⁺-ATPase from Sarcoplasmic Reticulum. *J. Biol. Chem.* **1989**, *264*, 4907–4915.
- (27) Brown, M. F. Soft Matter in Lipid-Protein Interactions. *Annu. Rev. Biophys.* **2017**, *46*, 379–410.
- (28) Brown, L. S. Eubacterial Rhodopsin - Unique Photosensors and Diverse Ion Pumps. *Biochim. Biophys. Acta, Bioenerg.* **2014**, *1837*, 553–561.
- (29) Govorunova, E. G.; Sineshchekov, O. A.; Li, H.; Spudich, J. L. Microbial Rhodopsins: Diversity, Mechanisms, and Optogenetic Applications. *Annu. Rev. Biochem.* **2017**, *86*, 845–872.
- (30) Pinhasi, J.; Delong, E. F.; Bějá, O.; González, J. M.; Pedrós-Alió, C. Marine Bacterial and Archaeal Ion-Pumping Rhodopsins: Genetic Diversity, Physiology, and Ecology. *Microbiol. Mol. Biol. Rev.* **2016**, *80*, 929–954.
- (31) Garavito, R. M.; Ferguson-Miller, S. Detergents as Tools in Membrane Biochemistry. *J. Biol. Chem.* **2001**, *276*, 32403–32406.
- (32) Möller, J. V.; Maire, M. Detergent Binding as a Measure of Hydrophobic Surface Area of Integral Membrane Proteins. *J. Biol. Chem.* **1993**, *268*, 18659–18672.
- (33) Casey, J. R.; Reithmeier, R. A. F. Detergent Interaction with Band 3, a Model Polytopic Membrane Protein. *Biochemistry* **1993**, *32*, 1172–1179.
- (34) Bějá, O.; Aravind, L.; Koonin, E. V.; Suzuki, M. T.; Hadd, A.; Nguyen, L. P.; Jovanovich, S. B.; Gates, C. M.; Feldman, R. A.; Spudich, J. L.; et al. Bacterial Rhodopsin: Evidence for a New Type of Phototrophy in the Sea. *Science* **2000**, *289*, 1902–1906.
- (35) Lakatos, M.; Lanyi, J. K.; Szakács, J.; Váró, G. The Photochemical Reaction Cycle of Proteorhodopsin at Low PH. *Biophys. J.* **2003**, *84*, 3252–3256.
- (36) Váró, G.; Brown, L. S.; Lakatos, M.; Lanyi, J. K. Characterization of the Photochemical Reaction Cycle of Proteorhodopsin. *Biophys. J.* **2003**, *84*, 1202–1207.
- (37) Ran, T.; Ozorowski, G.; Gao, Y.; Sineshchekov, O. A.; Wang, W.; Spudich, J. L.; Luecke, H. Cross-Protomer Interaction with the Photoactive Site in Oligomeric Proteorhodopsin Complexes. *Acta Crystallogr., Sect. D: Biol. Crystallogr.* **2013**, *69*, 1965–1980.
- (38) Henderson, L. J. Concerning the Relationship Between the Strength of Acids and Their Capacity to Preserve Neutrality. *Am. J. Physiol.* **1908**, *21*, 173–179.
- (39) Hasselbalch, K. A. Die Berechnung Der Wasserstoffzahl Des Blutes Aus Der Freien Und Gebundenen Kohlensäure Desselben, Und Die Sauerstoffbindung Des Blutes Als Funktion Der Wasserstoffzahl. *Biochem. Z.* **1917**, *78*, 112–144.
- (40) Maslennikov, I.; Kefala, G.; Johnson, C.; Riek, R.; Choe, S.; Kwiatkowski, W. NMR Spectroscopic and Analytical Ultracentrifuge Analysis of Membrane Protein Detergent Complexes. *BMC Struct. Biol.* **2007**, *7*, No. 74.
- (41) Heuberger, E. H. M. L.; Veenhoff, L. M.; Durkens, R. H.; Friesen, R. H. E.; Poolman, B. Oligomeric State of Membrane Transport Proteins Analyzed with Blue Native Electrophoresis and Analytical Ultracentrifugation. *J. Mol. Biol.* **2002**, *317*, 591–600.
- (42) Dioumaev, A. K.; Brown, L. S.; Shih, J.; Spudich, E. N.; Spudich, J. L.; Lanyi, J. K. Proton Transfers in the Photochemical Reaction Cycle of Proteorhodopsin. *Biochemistry* **2002**, *41*, 5348–5358.
- (43) Dioumaev, A. K.; Wang, J. M.; Bálint, Z.; Váró, G.; Lanyi, J. K. Proton Transport by Proteorhodopsin Requires That the Retinal Schiff Base Counterion Asp-97 Be Anionic. *Biochemistry* **2003**, *42*, 6582–6587.
- (44) Friedrich, T.; Geibel, S.; Kalmbach, R.; Chizhov, I.; Ataka, K.; Heberle, J.; Engelhard, M.; Bamberg, E. Proteorhodopsin Is a Light-Driven Proton Pump with Variable Vectoriality. *J. Mol. Biol.* **2002**, *321*, 821–838.
- (45) Hempelmann, F.; Hölper, S.; Verhoeven, M.-K.; Woerner, A. C.; Köhler, T.; Fiedler, S.-A.; Pfleger, N.; Wachtveitl, J.; Glaubitz, C. His75-Asp97 Cluster in Green Proteorhodopsin. *J. Am. Chem. Soc.* **2011**, *133*, 4645–4654.
- (46) Sharaabi, Y.; Brumfeld, V.; Sheves, M. Binding of Anions to Proteorhodopsin Affects the Asp97 pK_a. *Biochemistry* **2010**, *49*, 4457–4465.
- (47) Ranaghan, M. J.; Schwall, C. T.; Alder, N. N.; Birge, R. R. Green Proteorhodopsin Reconstituted into Nanoscale Phospholipid Bilayers (Nanodiscs) as Photoactive Monomers. *J. Am. Chem. Soc.* **2011**, *133*, 18318–18327.
- (48) Wang, J.; Link, S.; Heyes, C. D.; El-Sayed, M. A. Comparison of the Dynamics of the Primary Events of Bacteriorhodopsin in Its Trimeric and Monomeric States. *Biophys. J.* **2002**, *83*, 1557–1566.
- (49) Dencher, N. A.; Heyn, M. P. Formation and Properties of Bacteriorhodopsin Monomers in the Non-Ionic Detergents Octyl-Beta-D-Glucoside and Triton X-100. *FEBS Lett.* **1978**, *96*, 322–326.
- (50) Hussain, S.; Han, C.-t. Private communication.
- (51) Stoeckenius, W.; Wolff, E. K.; Hess, B. A Rapid Population Method for Action Spectra Applied to *Halobacterium halobium*. *J. Bacteriol.* **1988**, *170*, 2790–2795.
- (52) Dencher, N. A.; Heyn, M. P. Bacteriorhodopsin Monomers Pump Protons. *FEBS Lett.* **1979**, *108*, 307–310.
- (53) Kühlbrandt, W. Bacteriorhodopsin—the Movie. *Nature* **2000**, *406*, 569–570.

(54) Hussain, S.; Franck, J. M.; Han, S. Transmembrane Protein Activation Refined by Site-Specific Hydration Dynamics. *Angew. Chem., Int. Ed.* **2013**, *52*, 1953–1958.

(55) Chu, L. K.; El-Sayed, M. A. Kinetics of the M-Intermediate in the Photocycle of Bacteriorhodopsin upon Chemical Modification with Surfactants. *Photochem. Photobiol.* **2010**, *86*, 316–323.